Computational and Structural Biotechnology Journal 21 (2023) 5601–5608

Contents lists available at ScienceDirect

Computational and Structural Biotechnology Journal

journal homepage: www.elsevier.com/locate/csbj

Research article

Preoperative ^{18}F-FDG PET/CT and CT radiomics for identifying aggressive histopathological subtypes in early stage lung adenocarcinoma

Wookjin Choi [a,d,1], Chia-Ju Liu [b,1], Sadegh Riyahi Alam [a], Jung Hun Oh [a], Raj Vaghjiani [c], John Humm [a], Wolfgang Weber [b], Prasad S. Adusumilli [c], Joseph O. Deasy [a], Wei Lu [a,*]

[a] Department of Medical Physics, Memorial Sloan Kettering Cancer Center, New York, NY 10065, USA
[b] Department of Radiology, Memorial Sloan Kettering Cancer Center, New York, NY 10065, USA
[c] Department of Surgery, Memorial Sloan Kettering Cancer Center, New York, NY 10065, USA
[d] Department of Radiation Oncology, Thomas Jefferson University, Philadelphia, PA 19107, USA

ARTICLE INFO

Keywords:
Lung adenocarcinoma
Non-small cell lung cancer
Histopathology
Radiomics
PET
CT
Preoperative
Aggressive subtypes
Surgical planning

ABSTRACT

Lung adenocarcinoma (ADC) is the most common non-small cell lung cancer. Surgical resection is the primary treatment for early-stage lung ADC while lung-sparing surgery is an alternative for non-aggressive cases. Identifying histopathologic subtypes before surgery helps determine the optimal surgical approach. Predominantly solid or micropapillary (MIP) subtypes are aggressive and associated with a higher likelihood of recurrence and metastasis and lower survival rates. This study aims to non-invasively identify these aggressive subtypes using preoperative ^{18}F-FDG PET/CT and diagnostic CT radiomics analysis. We retrospectively studied 119 patients with stage I lung ADC and tumors $\leq$ 2 cm, where 23 had aggressive subtypes (18 solid and 5 MIPs). Out of 214 radiomic features from the PET/CT and CT scans and 14 clinical parameters, 78 significant features (3 CT and 75 PET features) were identified through univariate analysis and hierarchical clustering with minimized feature collinearity. A combination of Support Vector Machine classifier and Least Absolute Shrinkage and Selection Operator built predictive models. Ten iterations of 10-fold cross-validation (10 $\times$10-fold CV) evaluated the model. A pair of texture feature (PET GLCM Correlation) and shape feature (CT Sphericity) emerged as the best predictor. The radiomics model significantly outperformed the conventional predictor SUV_{max} (accuracy: 83.5% vs. 74.7%, p = 9e-9) and identified aggressive subtypes by evaluating FDG uptake in the tumor and tumor shape. It also demonstrated a high negative predictive value of 95.6% compared to SUV_{max} (88.2%, p = 2e-10). The proposed radiomics approach could reduce unnecessary extensive surgeries for non-aggressive subtype patients, improving surgical decision-making for early-stage lung ADC patients.

1. Introduction

Lung adenocarcinoma (ADC) is the most common histologic type of non-small cell lung cancer (NSCLC). Invasive ADC can be classified into five histopathologic subtypes based on their dominant growth patterns: lepidic, acinar, papillary, micropapillary (MIP), and solid [1], and Predominantly solid or MIP subtypes are aggressive with poorer prognosis, higher recurrence rate, vascular invasion, pleural invasion, lymph node, and distant metastasis [2–13]. The 2021 WHO Classification of Lung Tumors includes a new International Association for the Study of Lung Cancer (IASLC) grading system for invasive lung ADC based on the predominant histologic pattern of the tumor and the presence of high-grade components [14,15].

Surgical resection is the gold standard of treatment for early-stage NSCLC, with lobectomy being the standard mode of surgery since 1960 [16,17]. Advances in imaging and staging have allowed the detection of smaller tumors earlier, and rekindled interest in sublobar resection such as segmentectomy or wedge resection [18]. In two Phase III trials in patients clinically staged as T1N0 (tumor size $\leq$ 2 cm and pathologically confirmed node-negative), sublobar resection was found to be superior or not inferior to lobectomy with respect to disease-free and overall survival, though a two-fold increase in local relapses was reported in one trial [18,19]. Until now, there is no consensus on the appropriate indication for sublobar resection versus lobectomy in

* Correspondence to: Department of Medical Physics, Memorial Sloan Kettering Cancer Center, 500 Westchester Avenue, West Harrison, NY 10604, USA.
E-mail address: luw@mskcc.org (W. Lu).
[1] Both authors equally contributed to this work.

https://doi.org/10.1016/j.csbj.2023.11.008
Received 9 August 2023; Received in revised form 2 November 2023; Accepted 3 November 2023
Available online 4 November 2023

small-sized lung tumors [20–22]. Considering the worse prognosis of solid and MIP subtypes, lobectomy may be a more suitable option for patients with these aggressive subtypes [9,23].

Preoperative identification of aggressive subtypes could aid surgeons in selecting the optimal surgical procedures. Core biopsy has been used for identifying the dominant ADC subtype, which can be a prognostic factor for treatment response to stereotactic body radiation therapy [7]. However, core biopsy is an invasive procedure and can produce inconsistent results due to sampling errors [24].

Radiomic features extracted from medical images have shown promise in lung tissue classification, oncogenetics correlation, treatment response, and disease prognosis of lung cancer [25]. Using radiomic features from CT and PET/CT may provide a non-invasive preoperative method to identify those ADC subtypes with worse prognosis. CT radiomics can quantify the size, shape, margin, and internal density of tumors as imaging biomarkers of lung ADCs.

She et al. successfully differentiated indolent forms of adenocarcinoma from more invasive types, offering a potential tool for tailored interventions [26]. Fan et al. developed a radiomics signature to discern between invasive and non-invasive lesions, promising improved preoperative discrimination [27]. Park et al. leveraged a CT-based radiomic model to classify prognostic subtypes, showcasing its potential in refining adenocarcinoma classification. [28] Yang et al. recently introduced a CT-based nomogram for preoperative prediction of novel IASLC grading, demonstrating its utility in identifying high-grade ADCs and guiding treatment strategies [29]. These studies collectively highlight the significant role of radiomics in refining the assessment and management of lung ADCs.

Several studies have used CT features of ground-glass nodules (GGNs) to differentiate invasive ADC from pre-invasive lesions. For example, Lee et al. retrospectively investigated CT features for differentiating between invasive ADC and pre-invasive lesions appearing as GGNs. In pure GGNs, less than 10 mm lesion was a highly specific discriminator (sensitivity: 53.33%, specificity: 100%) [30]. In part-solid GGNs, pre-invasive lesions such as atypical adenomatous hyperplasia and adenocarcinoma in situ (AIS) were accurately identified (area under the curve [AUC]: 0.91) using the smaller lesion size, smaller solid proportion, non-lobulated border, and non-spiculated margin [30]. Son et al. claimed that quantitative analysis of preoperative CT imaging metrics could help distinguish invasive ADC from AIS or minimally invasive adenocarcinoma (AUC: 0.78) [31]. Chae et al. performed texture analysis to differentiate pre-invasive lesions from invasive ADC that manifest as part-solid GGNs. Higher kurtosis and smaller mass (adjusted odds ratios: 3.319 and 0.092, respectively) were significant predictors of pre-invasive lesions [32]. Furthermore, Song et al. predicted cases with MIP components greater than 5% of the entire tumor using tumor grade, sphericity, and entropy of co-occurrence matrix with an AUC of 0.61 [33].

PET/CT radiomics has emerged as a powerful tool in lung cancer research and management. The potential of quantitative image analysis for various aspects of lung cancer care has been explored, including computer-assisted diagnosis, survival prediction, and treatment response assessment. In particular, accurate identification of histologic subtype plays a pivotal role in shaping patient outcomes and guiding therapeutic decisions [34]. Ensuring the reproducibility and robustness of radiomics-derived features presents a critical challenge [35,36]. Variations from image acquisition, preprocessing, and tissue heterogeneity can introduce uncertainties. Standardized approaches in feature extraction and preprocessing are crucial for reliable radiomic analyses. Metrics like the Intraclass Correlation Coefficient (ICC), Overall Concordance Correlation Coefficient (OCCC), and Coefficient of Variations (COV) assess feature variability and robustness.

Studies have investigated lung adenocarcinoma growth patterns using radiomics. Shao et al. applied an ^{18}F-FDG PET/CT-based radiomics model to detect early invasive adenocarcinoma patterns. They analyzed 93 GGNs (lepidic, N = 18 and acinar-papillary, N = 75). Using selected radiomic features from both PET and CT scans, a rad-score was calculated, resulting in an AUC of 0.790, which is comparable to the AUC of 0.675 for the CT attenuation value of the ground-glass opacity component (CTGGO). The incorporation of rad-score with edge information in a joint model resulted in a minor improvement in AUC to 0.804. Their model combining CT parameters and PET/CT radiomics showed promise in predicting risk patterns and improving risk stratification and treatment planning [37]. Xiong et al. focused on identifying adenocarcinomas with lepidic growth in pure GGNs (>10 mm). By integrating clinical data, CT parameters, and radiomics, they improved identification. The radiomics-only and combined models outperformed the baseline model's AUC of 0.762 and the radiologist's highest AUC of 0.6, achieving test AUCs of 0.804 and 0.820, respectively [38].

This study aimed to identify early-stage lung ADC with aggressive subtypes, specifically predominant solid or MIP components, using preoperative ^{18}F-FDG PET/CT and CT radiomics analysis. To our knowledge, this is a pioneer radiomics study that combines the PET/CT and CT to address this important clinical question.

2. Materials and methods

Institutional Review Board approval was obtained for this retrospective study. Consecutive patients with preoperative CT and ^{18}F-FDG PET/CT between 2008 and 2011 were reviewed from the institution's database. Only patients with lung adenocarcinoma $\leq$ 2 cm on CT were included. Preoperative clinical risk factors including age, sex, smoking history, family history of lung cancer, prior malignancy history, and chronic obstructive pulmonary disease (COPD)/Emphysema were recorded. Histopathology subtyping of tumors was performed by experienced pathologists using hematoxylin and eosin-stained specimens according to the 2011 classification proposed by the IASLC, the American Thoracic Society (ATS), and the European Respiratory Society (ERS) [1]. The presence of lepidic, papillary, acinar, MIP, and solid components was documented in 5% increments, and the dominant subtype was defined as the morphologic component with the highest proportion. Tumors with MIP or solid pattern as the dominant component were labeled as aggressive subtypes. Table 1 provides a summary of patient characteristics. One patient was excluded from the analysis due to missing weight information needed to calculate standardized uptake values (SUV).

Helical CT images were obtained using a GE LightSpeed16 CT scanner (GE Healthcare, Chicago, IL) with the following parameters: tube voltage of 120kVp, current of 120–380 mA, and pitch of 0.984–1.750. The images were reconstructed to a 512 × 512 matrix with a slice thickness of 5 mm and pixel size ranging from 0.762 to 0.838 mm.

Table 1
Patient Characteristics.

Characteristic	Cohort (N = 120)
Age (years)	
Mean	67.0
Range	40–90
Sex, N (%)	
Male	46 (38.3%)
Female	74 (61.7%)
Histopathological subtype, N (%)	
Lepidic	37 (30.8%)
Acinar	47 (39.2%)
Papillary	12 (10.0%)
MIP	5 (4.2%)
Solid	19 (15.8%)
Aggressive subtypes (Solid+MIP)	24 (20.0%)
Clinical risk factors	
Smoking	100 (83.3%)
Family history of lung cancer	32 (26.7%)
Prior history of lung cancer	23 (19.2%)
Prior malignancy other than lung cancer	67 (55.8%)
COPD/Emphysema	14 (11.7%)

A physician visually reviewed the CT images for radiologic signs that may contribute to the prediction model, including tumor location (upper/middle lobe vs. lower lobe), pleural traction sign, tumor opacity (solid, part-solid, or ground-glass opacity), and speculated tumor margin. All PET/CT images were acquired using routine clinical protocol. Before the injection of FDG, the blood glucose of each patient was below 200 mg/dL after a 6-hour fasting period. All patients were scanned on a GE Discovery LS PET/CT system (GE Healthcare, Chicago, IL) 60 min after injection of 400–555 MBq FDG. PET images were reconstructed using the OSEM method to a 128 × 128 matrix with a slice thickness of 4.25 mm and pixel size of 3.9 mm. A low-dose CT scan (120–140 kV, 80 mA) was obtained and used for attenuation correction of the PET image data.

2.1. Tumor segmentation

Tumor segmentation was performed on both CT and PET/CT images. For CT, a nuclear medicine physician manually contoured the tumor on axial images. For PET/CT, a background subtracted lesion (BSL) segmentation method was used [39] (Fig. 1). This method estimates the background FDG uptake by fitting a Gaussian curve to the histogram from the area surrounding the tumor, and the tumor border is determined by thresholding at two standard deviations above the mean of background activity. The BSL method is suitable for small lesions and is relatively resistant to lung motion during PET acquisition [40]. The nuclear medicine physician (CL) reviewed the BSL segmentation results and occasionally made manual modifications for lesions with low FDG uptake. In some low FDG-avidity cases, the PET/CT segmentation may mistakenly connect to adjacent background activity such as mediastinum or liver, and the volume of interest used to initiate the BSL algorithm had to be repeatedly selected until the resultant segmentation closely matched the corresponding nodules on diagnostic CT. The segmentation was performed without knowledge of each case's clinical details and exact pathological subtypes.

2.2. Radiomic feature extraction

A total of 214 radiomic features were extracted from both diagnostic CT and ^{18}F-FDG-PET/CT images using PyRadiomics [41], with 107 features per scan. Furthermore, we utilized PyRadiomics [41] to extract filter-based features (Laplacian of Gaussian, Wavelet, Square, Square Root, Logarithm, Exponential, Gradient, Local Binary Pattern 2D and 3D), resulting in 1302 features for each scan and 2604 in total, leading to a grand total of 2818 features. Additionally, we extracted a set of 206 radiomic features from the same images with in-house software using the Insight Segmentation and Registration Toolkit (ITK) [42,43]. To correct for the partial volume effects (PVE) of the tumor in PET, the recovery coefficient method was used before calculating the maximum standardized uptake value (SUV_{max}) and radiomic features [44].

The PyRadiomics features comprise First Order Statistics, Shape-based 2D and 3D, Gray Level Co-occurrence Matrix (GLCM) [45], Gray Level Run Length Matrix (GLRLM) [46,47], Gray Level Size Zone Matrix (GLSZM) [48], Neighboring Gray Tone Difference Matrix (NGTDM) [49], and Gray Level Dependence Matrix (GLDM) [50]. These features characterized the intensity, shape, and texture of the tumor. First order statistics features quantified the level of intensity and distribution of voxel-wise CT attenuations or SUV of the PET/CT in a tumor. Shape features described geometric characteristics such as volume, diameter, elongation, and flatness of a tumor. Texture features quantified the spatial patterns of tissue density in CT or SUV in the PET/CT, such as homogeneity, coarseness, and correlation of intensity in a tumor, using GLCM, GLRLM, GLSZM, NGTDM, GLDM. The in-house radiomics quantified both diagnostic CT and PET/CT image intensities with normalization into 32 levels for contrast stretching due to the wide dynamic range of CT attenuation and continuous values of FDG uptake when constructing the GLCM and GLRM. The length of runs was

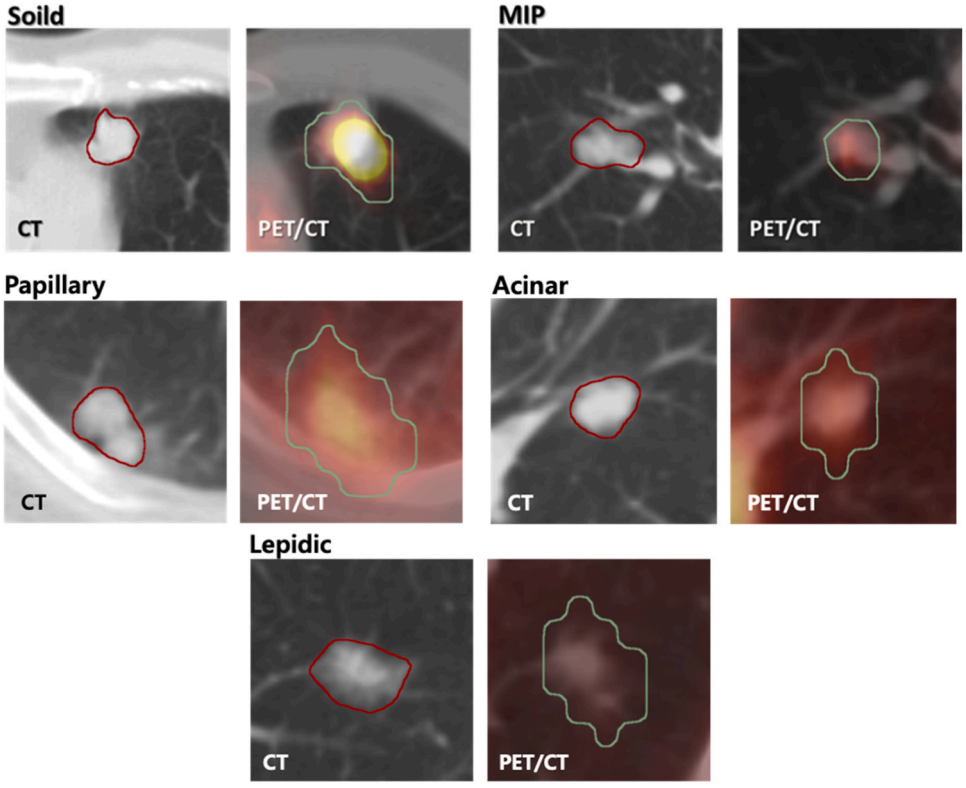

Fig. 1. Examples of the segmentation of aggressive types (solid and MIP) and other types (papillary, acinar, and lepidic) of invasive lung ADC on diagnostic CT and ^{18}F-FDG PET/CT. Red: the manual segmentation on diagnostic CT and Green: the automatic contour using background subtracted lesion (BSL) segmentation on FDG PET.

normalized by the diagonal length of the tumor's bounding box to make the GLRM scale-invariant. Finally, the average value of each texture feature was computed over all 13 spatial directions to obtain rotationally invariant features.

2.3. Prediction model

The prediction model integrated radiomic features and clinical parameters to identify tumors with aggressive subtypes. Three preprocessing steps were taken before constructing the prediction model to eliminate unnecessary features. Initially, we excluded unreliable radiomic features by employing intra-class correlation (ICC) to remove non-robust features. For this purpose, we applied supervoxel-based contour perturbation to each contour ten times. Subsequently, we calculated ICC1k (average absolute raters) and ICC2k (average random raters) and removed unreliable features by thresholding (ICC1k or ICC2k < 0.9).

Next, univariate analysis was applied to each radiomic feature, using the AUC of ROC and p-value computed by Wilcoxon rank-sum test. False discovery rate (FDR) correction was applied due to the multiple comparisons problem (q-value). The significant levels for both p-value and q-value are ≤ 0.05.

Finally, distinctive radiomic features were identified using the Ward's hierarchical clustering method [51]. The hierarchical feature cluster tree was divided into several prominent clusters (feature groups) by cutting at a threshold of the Spearman correlation coefficient $\rho \geq 0.7$. Distinctive features were selected as representative features with the smallest within-cluster correlation or as independent of all other features. Redundant features were removed from subsequent analysis.

The distinctive features chosen during the preprocessing were used to train a support vector machine (SVM) classifier using a 10-fold cross-validation (CV). Within each fold of the model building process, least absolute shrinkage and selection operator (LASSO) was used to rank and select important features using a nest 10-fold CV (inner-loop). An SVM classifier was then built to predict aggressive subtypes using a radial basis kernel function. The hyperparameters were optimized by using a grid search algorithm within combinations of $\gamma = \{0.0001, 0.001, 0.01, 0.1, 1, 10\}$ and C= {0.001, 0.01, 0.1, 1, 10, 100, 1000}. The outer loop was repeated ten times to obtain the model accuracy (10 ×10-fold CV). The 10 × 10 CV evaluated 100 models with different shuffled training and test datasets.

In each repetition, the patients were randomly divided into ten folds. One fold was selected as the test set, while the remaining nine folds were allocated to the training set. This process was repeated ten times by shuffling the entire dataset. To mitigate the effects of imbalanced data, we employed randomized oversampling to balance the training sets in the 10 × 10-fold CV.

During the SVM classifier training, we utilized the forward sequential feature selection (forward-SFS) method to choose ten different models that have from one optimal feature to ten optimal features. This method was based on the top ten most important features. These features were selected and ranked using the LASSO selection. The forward-SFS algorithm is a greedy method that iteratively identifies and adds the best new feature to a selected feature set. The procedure starts with no features and determines the most significant feature that maximizes the internal validation score when an estimator is trained on the single feature. After selecting the first feature, the process repeats by adding a new feature to the selected features. This process continues until ten features are included in the model. We also retain the optimal model at each number of features to compare model performance based on the number of features. When we add a new feature from the unselected feature list, we prioritize its importance according to the LASSO feature ranking. Finally, we chose models with ten different numbers of features.

3. Results

Among the 119 evaluable patients, 23 had aggressive subtypes (18 solid and 5 MIP). Table 2 shows the comparison of SUV_{max}, tumor size, and visual radiologic characteristics between aggressive and non-aggressive subtypes. There was no statistically significant difference between the two groups except for SUV_{max}, which had an AUC of 0.72 (q = 0.018). The mean SUV_{max} was higher for aggressive subtypes (8.1 ± 5.2) than non-aggressive subtypes (4.2 ± 2.8).

Univariate analysis revealed that 78 features were statistically significant predictors of outcome, including 3 CT features and 75 PET features. Table 3 shows the top 10 features were all derived from PET scans, comprising 6 texture features and 4 shape features. PET shape features provide a coarse shape analysis compared to CT shape features, due to the larger PET voxel size (4 mm). PET texture features analyze the patterns of FDG uptake in the PET scans. Specifically, GLCM Correlation measures linear dependencies between intensity levels. GLCM Cluster Shade quantifies skewness in the intensity distribution. Least Axis Length determines the smallest tumor diameter in 3D. GLDM Dependence Entropy evaluates randomness between neighboring voxels. GLRLM Run Length Non-Uniformity assesses variability in homogeneous tumor regions. Mesh Volume estimates the 3D surface that envelops the tumor. Voxel Volume sums the volume of significant voxels. Surface Area computes the 3D boundary area. GLSZM Small Area Low Gray Level Emphasis identifies small regions with low intensity. GLSZM Gray Level Non-Uniformity Normalized examines variations in intensity across tumor zones.

In multivariate analysis, the best SVM-LASSO model consisted of a pair of texture feature and shape feature: PET GLCM Correlation and CT Sphericity. PET GLCM Correlation is a measure of linear dependency of intensity levels, and it is high when high intensity levels are well distributed in a small region like a focal uptake in FDG PET. CT Sphericity quantifies the roundness of a shape in 3D CT by calculating how closely it approximates a sphere. The PET GLCM Correlation was significantly higher for aggressive subtypes (0.37 ± 0.3) than non-aggressive subtypes (0.11 ± 0.23), and CT Sphericity was higher for aggressive subtypes (0.69 ± 0.06) than non-aggressive subtypes (0.65 ± 0.08) as shown in Fig. 2. Table 4 shows the comparison of prediction accuracy using tumor size, SUV_{max}, and the SVM-LASSO model with three different feature sets (PyRadiomics – original image, PyRadiomics – including filtered images, and in-house radiomics tool). The SVM algorithm was used to create models based on tumor size and SUV_{max} without feature selection using LASSO. These models were subsequently compared to SVM-LASSO radiomics models for their predictive accuracy. We accomplished this by implementing 10 × 10-fold CV and hyperparameter optimization, with subsequent analysis conducted using the finalized model. The SVM-LASSO model with PyRadiomics features from original images had a sensitivity, specificity, positive predictive value (PPV), negative predictive value (NPV), and accuracy

Table 2
SUV_{max} and visual radiological predictors for predicting of aggressive lung ADC subtypes. Partial volume effect (PVE) was corrected using the recovery coefficient method.

Predictor	AUC	q-value	ρ
SUV_{max}	0.72	0.018	0.41
Tumor size	0.54	0.75	0.16
Location (upper 1/lower 0)	0.58	0.35	-0.13
Part-Solid	0.53	0.83	0.05
Spiculation	0.50	1.00	0.0007
Pleural	0.46	0.68	-0.07

AUC: area under the receiver operating characteristic curve, a plot of sensitivity and false positive rate (1 – specificity), q-value: False discovery rate adjusted Wilcoxon signed rank test p-value, ρ: Spearman correlation between the predictor and aggressive subtype.

Table 3
Top 10 important radiomics features obtained by univariate analysis for aggressive lung ADC.

	Type	Features	Categories	AUC	q-value	ρ
1	PET	GLCM Correlation	Texture	0.79	0.0017	0.39
2	PET	GLCM Cluster Shade	Texture	0.78	0.0026	0.38
3	PET	Least Axis Length	Shape	0.77	0.0030	0.42
4	PET	GLDM Dependence Entropy	Texture	0.76	0.0036	0.35
5	PET	GLRLM Run Length Non Uniformity	Texture	0.75	0.0043	0.41
6	PET	Mesh Volume	Shape	0.75	0.0046	0.43
7	PET	Voxel Volume	Shape	0.75	0.0046	0.44
8	PET	Surface Area	Shape	0.75	0.0046	0.43
9	PET	GLSZM Small Area Low Gray Level Emphasis	Texture	0.75	0.0047	-0.27
10	PET	GLSZM Gray Level Non Uniformity Normalized	Texture	0.75	0.0047	-0.27

AUC: area under the receiver operating characteristic curve, a plot of sensitivity and false positive rate (1 – specificity), q-value: False discovery rate adjusted Wilcoxon signed rank test p-value, ρ: Spearman correlation between the predictor and aggressive subtype.

with the 10 × 10-fold CV of 84.1%, 83.3%, 55.0%, 95.6%, and 83.5%, respectively. All were significantly higher than those of SUV_{max} (55.7%, 79.3%, 39.2%, 88.2%, and 74.7%, respectively) or tumor size (40.4%, 56.3%, 18.3, 79.6%, and 53.2%, respectively). Adding more than two features to the models decreased their accuracy. SVM-LASSO using the other feature sets (PyRadiomics features including filtered images and our in-house radiomics tool) showed lower performance than the best model, but still significantly higher than SUV_{max}. Statistical tests were utilized to evaluate diagnostic test performance. The McNemar test, for paired nominal data, was utilized to analyze sensitivity, specificity, and accuracy, providing insights into the marginal homogeneity of two dichotomous variables. [52]. In addition, the Moskowitz and Pepe test was employed to compare PPV and NPV, giving a comprehensive evaluation of the predictive power of the diagnostic tests [53]. Differential AUCs were assessed using DeLong's ROCs test, which demonstrated the discriminatory capabilities of the analyzed techniques [54].

Table 5 illustrates that the best SVM-LASSO model for predicting the solid subtype had an accuracy of 80.6 ± 1.5%, sensitivity of 82.7 ± 6.4%, and specificity of 80.3 ± 2.0% using the same features (PET GLCM Correlation and CT Sphericity). However, the identification of the MIP subtype using radiomics was challenging, with a much lower PPV of 42.0 ± 2.5% and a large variation in sensitivity of 86.0 ± 16.5%.

4. Discussion

The appropriate selection of lobectomy vs. sublobar resection for early lung ADC remains an area of debate [55]. Sublobar resections preserve more lung reserve, while lobectomy provides better parenchymal margins and lymphatic clearance. Sublobar resection is reasonable for tumors ≤ 2 cm. However, higher rates of lymph node metastases have been noticed in tumors with solid or MIP subtypes, even when the tumor sizes are small [56–58]. Thus, lobectomy is more favored for tumors with solid or MIP subtypes [58]. The dilemma of resection methods for small lung tumors highlights the importance of histopathological subtyping of lung ADC before surgical resection.

There are few studies that predict lung ADC subtypes before tumor resection. The SUV_{max} of PET has been shown to have a close association with lung ADC subtypes and grading. MIP and solid subtypes tend to have higher SUV_{max} than the other subtypes [59–62]. However, the discriminative power of SUV_{max} is inevitably limited by the partial volume effect for small tumors [44], and as a single-point estimate, SUV_{max} fails to characterize intratumoral heterogeneity [63–65]. Despite the important role of PET in the diagnosis and staging of lung ADC, it has been reported that false negative results are common in tumors ≤ 2 cm [66]. The tumor-size-dependent sensitivity of PET may explain the improved but still low sensitivity and PPV of our models. Our radiomics model achieved high specificity, high NPV, and good accuracy in predicting aggressive subtypes of lung ADC. Compared with the SUV_{max} based SVM model, the SVM-LASSO model using PET GLCM Correlation and CT Sphericity significantly improved accuracy (Table 4).

The accuracy of our model relied heavily on its ability to identify the solid subtype, rather than the MIP subtype because the number of the MIP subtype cases is much smaller. The compact sheets of malignant cells and lack of alveolar space in the solid subtype make its spatial structure distinct from the other four subtypes. Univariate analysis revealed that 99 radiomic features were significant in predicting the solid subtype (7 CT, 92 PET, and none of the clinical parameters, with an AUC of 0.68–0.83), but no feature was significant in predicting the MIP subtype although the AUC for the best 10 features of the MIP subtype (0.86–0.90) is higher than that of the solid subtype.

Meanwhile, SVM-LASSO identified three features (2nd Cancer, PET GLCM Correlation, and PET GLSZM Small Area Low Gray Level Emphasis) that can accurately predict MIP dominant subtypes with a high accuracy of 87.2% as shown in Table 5. The limited number of MIP cases and their low representation in the training set, compounded by the intratumoral heterogeneity of growth patterns, posed challenges in accurately capturing MIP subregions during model building. Consequently, sensitivity exhibited significant variability and PPV demonstrated lower performance. Additionally, the fine structural distinctions

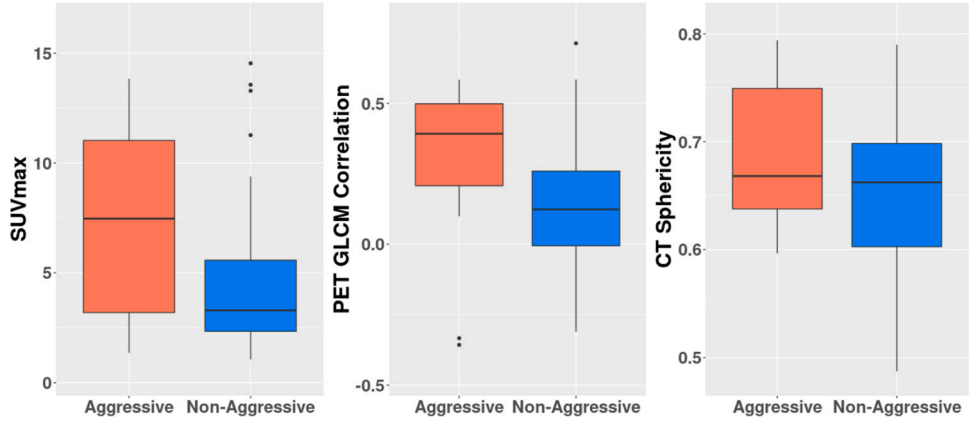

Fig. 2. The box plots depicting SUV_{max} (q=0.018), PET GLCM Correlation (q=0.0017) and CT Shape Sphericity (q=0.18) demonstrate significant differences between aggressive and non-aggressive subtypes. The median is indicated by the central mark.

Table 4
Accuracy of the Tumor Size, SUV_{max} and SVM-LASSO models with different feature sets to predict aggressive lung ADC. All the metrics were obtained through the 10 × 10-fold cross-validation.

	Sensitivity	Specificity	PPV	NPV	Accuracy	AUC
a. Conventional Tumor Size	40.4 ± 5.5%	56.3 ± 2.0%	18.3 ± 2.6%	79.6 ± 1.4%	53.2 ± 1.9%	0.60 ± 0.05
b. Conventional SUV_{max}	55.7 ± 1.8%	79.3 ± 1.1%	39.2 ± 2.0%	88.2 ± 0.6%	74.7 ± 1.2%	0.64 ± 0.01
c. SVM-LASSO PyRadiomics original only	**84.1 ± 5.9%**	83.3 ± 2.3%	**55.± 1.6%**	**95.6 ± 3.7%**	**83.5 ± 2.2%**	**0.84 ± 0.03**
p-value b vs. c	5e-10	0.04	3e-8	2e-10	9e-9	0.001
d. SVM-LASSO PyRadiomics with filters	63.0 ± 6.5%	85.0 ± 2.2%	50.3 ± 5.1%	90.6 ± 1.6%	80.8 ± 2.6%	0.79 ± 0.02
p-value b vs. d	0.02	0.003	2e-4	0.02	2e-4	0.04
e. SVM-LASSO in-house radiomics	67.4 ± 3.1%	**86.0 ± 1.1%**	53.7 ± 2.1%	91.7 ± 1.0%	82.4 ± 1.0%	0.78 ± 0.01
p-value b vs. e	6e-6	6e-5	2e-8	7e-8	1e-8	0.01
	Selected Features of the SVM-LASSO model					N
c.	PET GLCM Correlation, CT Shape Sphericity					2
d.	CT Logarithm GLDM Large Dependence High Gray Level Emphasis, PET LBP2D Firstorder Total Energy, PET Wavelet LHL GLCM Cluster Shade, PET Logarithm GLCM Contrast, CT Wavelet LLH Firstorder Maximum					5
e.	PET Mean of Cluster Shade					1

PPV: positive predictive value, NPV: negative predictive value, AUC: area under the receiver operating characteristic curve, a plot of sensitivity and false positive rate (1 – specificity), p-value: McNemar test for sensitivity, specificity, and accuracy comparison, Moskowitz and Pepe test for PPV and NPV comparison, DeLong's ROCs test for AUC comparison, N: the number of the selected features.

Table 5
Accuracy of the SVM-LASSO models for the prediction of solid and MIP dominant lung ADC respectively, and selected features.

Subtype	Sensitivity	Specificity	PPV	NPV	Accuracy	AUC
Solid (N = 18)	82.7 ± 6.4%	80.3 ± 2.0%	42.0 ± 2.5%	96.4 ± 1.3%	80.6 ± 1.5%	0.82 ± 0.03
	PET GLCM Correlation, CT Shape Sphericity					
MIP (N = 5)	86.0 ± 16.5%	87.2 ± 2.1%	23.2 ± 4.1%	99.2 ± 0.9%	87.2 ± 2.3%	0.87 ± 0.09
	2nd Cancer, **PET GLCM Correlation**, PET GLSZM Small Area Low Gray Level Emphasis					

PPV: positive predictive value, NPV: negative predictive value, AUC: area under the receiver operating characteristic curve, a plot of sensitivity and false positive rate (1 – specificity)

between MIP tufts and papillary fibrovascular cores, discernible under high-power filed microscope with a 0.2 μm resolution, are beyond the capability of texture features derived from PET/CT, which operates at a much coarser resolution (3–5 mm). Further dedicated research on MIP is imperative to enhance outcomes for patients with MIP-dominant ADC and address its poor prognosis.

CT has traditionally been the primary diagnostic tool for lung cancer, as small lung ADCs can exhibit diverse sizes, shapes, margins, and internal densities (non-solid, part-solid to mostly solid) [67]. Although CT texture analysis has been used for prognostic stratification by identifying invasive lung ADC among GGNs [30,31] or among part-solid nodules [32], our study found that none of the CT features were as effective as PET features in predicting solid and MIP subtypes in the univariate analysis. However, CT Sphericity was selected as the second feature along with PET GLCM Correlation in SVM-LASSO model to complement PET texture feature.

Currently, lung ADC subtyping using preoperative core biopsy sampling or intraoperative frozen section is not routinely performed due to increased cost and invasiveness, which can result in sampling errors [68,69]. In contrast, imaging phenotype analysis as a biomarker for lung ADC histology has the advantages of being non-invasive and cost-effective. Our study used preoperative imaging modalities to build the prediction model, enabling the evaluation of the entire tumor to avoid sampling errors. Previous studies have also used imaging features to predict aggressive subtypes of ADC, with Song et al. describing the CT characteristics of MIP as more homogenous and less spherical periphery than solid [33], and Yang et al. demonstrating high accuracy of CT radiomics in predicting solid and MIP subtypes with sensitivity, specificity, and accuracy of 83.3%, 98.7%, and 91.6%, respectively [70]. However, Yang's model only analyzed tumors with a high percentage (>70%) of dominant histopathological subtype, and their results may not be applicable to tumors with < 70% of dominant histopathological subtype.

The large difference between the resolutions of PET/CT images (3–5 mm) and light microscope (0.2 μm) may have compromised the accuracy of prediction models. The interspersed distribution of aggressive subtypes in the tumor also limit the sensitivity of the model, as well as other conventional indicators such as solid component on CT, SUV_{max} of PET, and preoperative core biopsy. Due to the unsatisfactory PPV of 55.0%, the model cannot aid surgeons in selecting lobectomy for a patient who is predicted as aggressive subtype. However, with a high NPV of 95.67%, the model may aid surgeons in selecting sublobar resection for a patient who is predicted as non-aggressive subtype.

The study was limited by the modest patient cohort and retrospective nature. Manual segmentation of tumors on CT can suffer significant inter- and intra-observer variability. Although automatic segmentation algorithms may be technically difficult due to the indistinct and fuzzy borders of these small tumors, they may be worth exploring in future studies. Another limitation is that all patients were recruited from one cancer institute, resulting in a higher prevalence of patients with prior lung cancer, malignancy, or family history of lung cancer than the general population. The variance or inconsistency between different institutes should be validated in a multi-institute study.

5. Conclusion

In conclusion, we developed a radiomics model to predict aggressive subtypes of lung ADC using preoperative ^{18}F-FDG PET/CT and

diagnostic CT. The model achieved an accuracy of 83.5% with good sensitivity of 84.1%, high specificity of 83.3%, and high NPV of 95.6%. The proposed radiomics approach with high NPV can help surgeons improve surgical decision-making in patients with early lung ADC to avoid unnecessary extensive surgery such as lobectomy in patients with non-aggressive subtypes suitable for sublobar resection.

CRediT authorship contribution statement

Wookjin Choi: Conceptualization, Methodology, Software, Writing - original draft. Chia-Ju Liu: Conceptualization, Data curation, Writing - original draft. Sadegh Riyahi Alam: Investigation, Validation, Writing - review & editing. Jung Hun Oh: Investigation, Validation, Writing - review & editing. Raj Vaghjiani: Investigation, Validation, Writing - review & editing. John Humm: Investigation, Resources, Writing - review & editing. Wolfgang Weber: Investigation, Resources, Writing - review & editing. Prasad S. Adusumilli: Conceptualization, Supervision, Resources, Writing - review & editing. Joseph O. Deasy: Supervision, Resources, Writing - review & editing. Wei Lu: Funding acquisition, Conceptualization, Methodology, Writing - original draft.

Declaration of Competing Interest

This work was supported in part by the NIH/NCI Grant No. R01 CA172638 and the NIH/NCI Cancer Center Support Grant P30 CA008748 and 5P30 CA056036. The authors have no relevant conflicts of interest to disclose.

Acknowledgements

This work was supported in part by the NIH/NCI Grant No. R01 CA172638, and the NIH/NCI Cancer Center Support Grant No. P30 CA008748 and 5P30 CA056036.

References

[1] Travis WD, et al. International association for the study of lung cancer/american thoracic society/european respiratory society international multidisciplinary classification of lung adenocarcinoma (in eng) J Thorac Oncol: Publ Int Assoc Study Lung Cancer 2011;vol. 6(2):244–85. https://doi.org/10.1097/JTO.0b013e318206a221.

[2] Russell PA, Wainer Z, Wright GM, Daniels M, Conron M, Williams RA. Does lung adenocarcinoma subtype predict patient survival?: A clinicopathologic study based on the new International Association for the Study of Lung Cancer/American Thoracic Society/European Respiratory Society international multidisciplinary lung adenocarcinoma classification. J Thorac Oncol: Publ Int Assoc Study Lung Cancer 2011;vol. 6(9):1496–504. https://doi.org/10.1097/JTO.0b013e318221f701.

[3] Warth A, et al. The novel histologic International Association for the Study of Lung Cancer/American Thoracic Society/European Respiratory Society classification system of lung adenocarcinoma is a stage-independent predictor of survival. J Clin Oncol 2012;vol. 30(13):1438–46. https://doi.org/10.1200/JCO.2011.37.2185.

[4] Yanagawa N, Shiono S, Abiko M, Ogata SY, Sato T, Tamura G. The correlation of the International Association for the Study of Lung Cancer (IASLC)/American Thoracic Society (ATS)/European Respiratory Society (ERS) classification with prognosis and EGFR mutation in lung adenocarcinoma. Ann Thorac Surg 2014;vol. 98(2):453–8. https://doi.org/10.1016/j.athoracsur.2014.04.108.

[5] Morales-Oyarvide V, Mino-Kenudson M. High-grade lung adenocarcinomas with micropapillary and/or solid patterns: a review. Curr Opin Pulm Med 2014;vol. 20(4):317–23. https://doi.org/10.1097/MCP.0000000000000070.

[6] Bains S, et al. Procedure-specific risk prediction for recurrence in patients undergoing lobectomy or sublobar resection for small (</=2 cm) lung adenocarcinoma: an international cohort analysis. J Thorac Oncol: Publ Int Assoc Study Lung Cancer 2019;vol. 14(1):72–86. https://doi.org/10.1016/j.jtho.2018.09.008.

[7] Leeman JE, et al. Histologic subtype in core lung biopsies of early-stage lung adenocarcinoma is a prognostic factor for treatment response and failure patterns after stereotactic body radiation therapy (in eng) Int J Radiat Oncol Biol Phys 2017;vol. 97(1):138–45. https://doi.org/10.1016/j.ijrobp.2016.09.037.

[8] Ujiie H, et al. Solid predominant histologic subtype in resected stage i lung adenocarcinoma is an independent predictor of early, extrathoracic, multisite recurrence and of poor postrecurrence survival. Sep 10 J Clin Oncol 2015;vol. 33(26):2877–84. https://doi.org/10.1200/JCO.2015.60.9818.

[9] Nitadori J, et al. Impact of micropapillary histologic subtype in selecting limited resection vs lobectomy for lung adenocarcinoma of 2cm or smaller. Aug 21 J Natl Cancer Inst 2013;vol. 105(16):1212–20. https://doi.org/10.1093/jnci/djt166.

[10] Bao F, Yuan P, Yuan X, Lv X, Wang Z, Hu J. Predictive risk factors for lymph node metastasis in patients with small size non-small cell lung cancer. J Thorac Dis 2014;vol. 6(12):1697–703. https://doi.org/10.3978/j.issn.2072-1439.2014.11.05.

[11] Hung JJ, et al. Prognostic factors of survival after recurrence in patients with resected lung adenocarcinoma. J Thorac Oncol: Publ Int Assoc Study Lung Cancer 2015;vol. 10(9):1328–36. https://doi.org/10.1097/JTO.0000000000000618.

[12] Yeh YC, et al. International association for the study of lung cancer/american thoracic society/european respiratory society classification predicts occult lymph node metastasis in clinically mediastinal node-negative lung adenocarcinoma. Eur J Cardiothorac Surg 2016;vol. 49(1):e9–15. https://doi.org/10.1093/ejcts/ezv316.

[13] Takahashi Y, et al. Preponderance of high-grade histologic subtype in autologous metastases in lung adenocarcinoma. Mar 15 Am J Respir Crit Care Med 2018;vol. 197(6):816–8. https://doi.org/10.1164/rccm.201705-0924LE.

[14] Nicholson AG, et al. The 2021 WHO classification of lung tumors: impact of advances since 2015. 2022-03-01 J Thorac Oncol 2022;vol. 17(3):362–87. https://doi.org/10.1016/j.jtho.2021.11.003.

[15] Moreira AL, et al. A grading system for invasive pulmonary adenocarcinoma: a proposal from the international association for the study of lung cancer pathology committee. 2020-10-01 J Thorac Oncol 2020;vol. 15(10):1599–610. https://doi.org/10.1016/j.jtho.2020.06.001.

[16] Cahan WG. Radical lobectomy. J Thorac Cardiovasc Surg 1960;vol. 39:555–72 ([Online]. Available), ⟨https://www.ncbi.nlm.nih.gov/pubmed/13806783⟩.

[17] Harpole Jr DH, Herndon 2nd JE, Young Jr WG, Wolfe WG, Sabiston Jr DC. Stage I nonsmall cell lung cancer. A multivariate analysis of treatment methods and patterns of recurrence. Sep 1 Cancer 1995;vol. 76(5):787–96. Sep 1, ⟨https://www.ncbi.nlm.nih.gov/pubmed/8625181⟩.

[18] Altorki N, et al. Lobar or sublobar resection for peripheral stage IA non–small-cell lung cancer. N Engl J Med 2023;vol. 388(6):489–98. https://doi.org/10.1056/nejmoa2212083.

[19] Saji H, et al. Segmentectomy versus lobectomy in small-sized peripheral non-small-cell lung cancer (JCOG0802/WJOG4607L): a multicentre, open-label, phase 3, randomised, controlled, non-inferiority trial. Lancet 2022;vol. 399(10335):1607–17. https://doi.org/10.1016/S0140-6736(21)02333-3.

[20] Hattori A, et al. Is limited resection appropriate for radiologically "solid" tumors in small lung cancers? Ann Thorac Surg 2012;vol. 94(1):212–5. https://doi.org/10.1016/j.athoracsur.2012.03.033.

[21] Hattori A, Suzuki K, Matsunaga T, Miyasaka Y, Takamochi K, Oh S. What is the appropriate operative strategy for radiologically solid tumours in subcentimetre lung cancer patients?dagger. Eur J Cardiothorac Surg 2015;vol. 47(2):244–9. https://doi.org/10.1093/ejcts/ezu250.

[22] Hennon M, Landreneau RJ. Role of segmentectomy in treatment of early-stage non-small cell lung cancer. Ann Surg Oncol 2018;vol. 25(1):59–63. https://doi.org/10.1245/s10434-017-5787-5.

[23] Kadota K, et al. Tumor spread through air spaces is an important pattern of invasion and impacts the frequency and location of recurrences after limited resection for small stage i lung adenocarcinomas. J Thorac Oncol: Publ Int Assoc Study Lung Cancer 2015;vol. 10(5):806–14. https://doi.org/10.1097/JTO.0000000000000486.

[24] Matsuzawa R, et al. Factors influencing the concordance of histological subtype diagnosis from biopsy and resected specimens of lung adenocarcinoma. Lung Cancer (Amst, Neth) 2016;vol. 94:1–6. https://doi.org/10.1016/j.lungcan.2016.01.009.

[25] Bashir U, Siddique MM, McLean E, Goh V, Cook GJ. Imaging heterogeneity in lung cancer: techniques, applications, and challenges. Ajr Am J Roentgenol 2016;vol. 207(3):534–43. https://doi.org/10.2214/AJR.15.15864.

[26] She Y, et al. The predictive value of CT-based radiomics in differentiating indolent from invasive lung adenocarcinoma in patients with pulmonary nodules. 2018-12-01 Eur Radiol 2018;vol. 28(12):5121–8. https://doi.org/10.1007/s00330-018-5509-9.

[27] Fan L, et al. Radiomics signature: a biomarker for the preoperative discrimination of lung invasive adenocarcinoma manifesting as a ground-glass nodule. 2019-02-01 Eur Radiol 2019;vol. 29(2):889–97. https://doi.org/10.1007/s00330-018-5530-z.

[28] Park S, et al. Differentiation of predominant subtypes of lung adenocarcinoma using a quantitative radiomics approach on CT. 2020-09-01 Eur Radiol 2020;vol. 30(9):4883–92. https://doi.org/10.1007/s00330-020-06805-w.

[29] Yang Z, et al. A CT-based radiomics nomogram combined with clinic-radiological characteristics for preoperative prediction of the novel IASLC grading of invasive pulmonary adenocarcinoma. Acad Radiol 2023;vol. 30(9):1946–61. https://doi.org/10.1016/j.acra.2022.12.006.

[30] Lee SM, Park CM, Goo JM, Lee HJ, Wi JY, Kang CH. Invasive pulmonary adenocarcinomas versus preinvasive lesions appearing as ground-glass nodules: differentiation by using CT features. Radiology 2013;vol. 268(1):265–73. https://doi.org/10.1148/radiol.13120949.

[31] Son JY, et al. Quantitative CT analysis of pulmonary ground-glass opacity nodules for the distinction of invasive adenocarcinoma from pre-invasive or minimally invasive adenocarcinoma. PloS One 2014;vol. 9(8):e104066. https://doi.org/10.1371/journal.pone.0104066.

[32] Chae HD, Park CM, Park SJ, Lee SM, Kim KG, Goo JM. Computerized texture analysis of persistent part-solid ground-glass nodules: differentiation of preinvasive lesions from invasive pulmonary adenocarcinomas (in eng) Radiology 2014;vol. 273(1):285–93. https://doi.org/10.1148/radiol.14132187.

[33] Song SH, et al. Imaging phenotyping using radiomics to predict micropapillary pattern within lung adenocarcinoma (in eng) J Thorac Oncol: Publ Int Assoc Study Lung Cancer 2017;vol. 12(4):624–32. https://doi.org/10.1016/j.jtho.2016.11.2230.
[34] Bianconi F, Palumbo I, Spanu A, Nuvoli S, Fravolini ML, Palumbo B. PET/CT radiomics in lung cancer: an overview. 2020-03-03 Appl Sci 2020;vol. 10(5):1718. https://doi.org/10.3390/app10051718.
[35] Hosseini SA, Shiri I, Hajianfar G, Ghafarian P, Bakhshayesh Karam M, Ay MR. The impact of preprocessing on the PET-CT radiomics features in non-small cell lung cancer. 2021-11-15 Front Biomed Technol 2021. https://doi.org/10.18502/fbt.v8i4.7754.
[36] Hosseini SA, et al. "Synergistic impact of motion and acquisition/reconstruction parameters on 18F-FDG PET radiomic features in non-small cell lung cancer: Phantom and clinical studies. 2022-06-01 Med Phys 2022;vol. 49(6):3783–96. https://doi.org/10.1002/mp.15615.
[37] Shao X, Niu R, Shao X, Jiang Z, Wang Y. "Value of 18F-FDG PET/CT-based radiomics model to distinguish the growth patterns of early invasive lung adenocarcinoma manifesting as ground-glass opacity nodules,". 2020-12-01 EJNMMI Res 2020;vol. 10(1). https://doi.org/10.1186/s13550-020-00668-4.
[38] Xiong Z, et al. Radiomics for identifying lung adenocarcinomas with predominant lepidic growth manifesting as large pure ground-glass nodules on CT images. 2022-06-24 PloS One 2022;vol. 17(6):e0269356. https://doi.org/10.1371/journal.pone.0269356.
[39] Burger IA, et al. PET quantification with a histogram derived total activity metric: superior quantitative consistency compared to total lesion glycolysis with absolute or relative SUV thresholds in phantoms and lung cancer patients. 2014 May-Jun " (Eng), Nucl Med Biol 2014;vol. 41(5):410–8. https://doi.org/10.1016/j.nucmedbio.2014.02.006.
[40] Li G, Schmidtlein CR, Burger IA, Ridge CA, Solomon SB, Humm JL. Assessing and accounting for the impact of respiratory motion on FDG uptake and viable volume for liver lesions in free-breathing PET using respiration-suspended PET images as reference. Med Phys 2014;vol. 41(9):091905. https://doi.org/10.1118/1.4892602.
[41] van Griethuysen JJM, et al. Computational radiomics system to decode the radiographic phenotype. Nov 1 Cancer Res 2017;vol. 77(21):e104–7. https://doi.org/10.1158/0008-5472.CAN-17-0339.
[42] Choi W, Nadeem S, Alam SR, Deasy JO, Tannenbaum A, Lu W. Reproducible and interpretable spiculation quantification for lung cancer screening. Comput Methods Prog Biomed 2021;vol. 200. https://doi.org/10.1016/j.cmpb.2020.105839.
[43] Choi W, et al. Radiomics analysis of pulmonary nodules in low-dose CT for early detection of lung cancer. Med Phys 2018;vol. 45(4). https://doi.org/10.1002/mp.12820.
[44] Soret M, Bacharach SL, Buvat I. Partial-volume effect in PET tumor imaging. J Nucl Med: Publ, Soc Nucl Med 2007;vol. 48(6):932–45. https://doi.org/10.2967/jnumed.106.035774.
[45] Haralick RM, Shanmugam K, Dinstein I. Textural features for image classification (in English) IEEE T Syst Man Cyb 1973;vol. Smc3(6):610–21. https://doi.org/10.1109/Tsmc.1973.4309314.
[46] Galloway MM. Texture analysis using gray level run lengths. Comput Graph Image Process 1975;vol. 4(2):172–9.
[47] Tang XO. Texture information in run-length matrices (in English) IEEE T Image Process 1998;vol. 7(11):1602–9. https://doi.org/10.1109/83.725367.
[48] G. Thibault, B. Fertil, and C. Navarro, "Texture indexes and gray level size zone matrix: appli-cation to cell nuclei classification in Proceedings of the Pattern Recognition and Information Processing 2009," in International Conference on Pattern Recognition and Information Processing (PRIP'09), pp. 140–145.
[49] Amadasun M, King R. Textural features corresponding to textural properties. IEEE Trans Syst, Man, Cybern 1989;vol. 19(5):1264–74. https://doi.org/10.1109/21.44046.
[50] Chengjun S, William GW. Neighboring gray level dependence matrix for texture classification. Comput Vis, Graph, Image Process 1983;vol. 23(3):341–52. https://doi.org/10.1016/0734-189X(83)90032-4.
[51] Ward Jr JH. Hierarchical grouping to optimize an objective function. J Am Stat Assoc 1963;Vol. 58(No. 301):236–44.
[52] McNemar Q. Note on the sampling error of the difference between correlated proportions or percentages. Psychometrika 1947;vol. 12(2):153–7. https://doi.org/10.1007/BF02295996.
[53] Moskowitz CS, Pepe MS. "Comparing the predictive values of diagnostic tests: sample size and analysis for paired study designs (in eng) Clin Trials 2006;vol. 3(3):272–9. https://doi.org/10.1191/1740774506cn147oa.
[54] DeLong ER, DeLong DM, Clarke-Pearson DL. Comparing the areas under two or more correlated receiver operating characteristic curves: a nonparametric approach (in eng) Biometrics 1988;vol. 44(3):837–45. ⟨https://www.ncbi.nlm.nih.gov/pubmed/3203132⟩.
[55] Berfield KS, Wood DE. "Sublobar resection for stage IA non-small cell lung cancer,". J Thorac Dis 2017;vol. 9(Suppl 3):S208–10. https://doi.org/10.21037/jtd.2017.03.135.
[56] Haruki T, et al. Clinicopathological Characteristics of Lung Adenocarcinoma with Unexpected Lymph Node Metastasis. Aug 20 Ann Thorac Cardiovasc Surg 2017;vol. 23(4):181–7. https://doi.org/10.5761/atcs.oa.16-00309.
[57] Yu Y, Jian H, Shen L, Zhu L, Lu S. Lymph node involvement influenced by lung adenocarcinoma subtypes in tumor size </=3 cm disease: A study of 2268 cases. Eur J Surg Oncol 2016;vol. 42(11):1714–9. https://doi.org/10.1016/j.ejso.2016.02.247.
[58] Wang L, et al. Lymph node metastasis in clinical stage IA peripheral lung cancer. Lung Cancer (Amst, Neth) 2015;vol. 90(1):41–6. https://doi.org/10.1016/j.lungcan.2015.07.003.
[59] Nakamura H, et al. Close association of IASLC/ATS/ERS lung adenocarcinoma subtypes with glucose-uptake in positron emission tomography. Lung Cancer (Amst, Neth) 2015;vol. 87(1):28–33. https://doi.org/10.1016/j.lungcan.2014.11.010.
[60] Cha MJ, et al. Micropapillary and solid subtypes of invasive lung adenocarcinoma: clinical predictors of histopathology and outcome. e2, Mar " (Eng), J Thorac Cardiovasc Surg 2014;vol. 147(3):921–8. https://doi.org/10.1016/j.jtcvs.2013.09.045.
[61] Lee HY, et al. Histopathology of lung adenocarcinoma based on new IASLC/ATS/ERS classification: prognostic stratification with functional and metabolic imaging biomarkers. J Magn Reson Imaging 2013;vol. 38(4):905–13. https://doi.org/10.1002/jmri.24080.
[62] Kadota K, et al. FDG-PET SUVmax combined with IASLC/ATS/ERS histologic classification improves the prognostic stratification of patients with stage I lung adenocarcinoma. Ann Surg Oncol 2012;vol. 19(11):3598–605. https://doi.org/10.1245/s10434-012-2414-3.
[63] Tan S, et al. "Spatial-temporal [(1)(8)F]FDG-PET features for predicting pathologic response of esophageal cancer to neoadjuvant chemoradiation therapy,". Apr 1 Int J Radiat Oncol Biol Phys 2013;vol. 85(5):1375–82. https://doi.org/10.1016/j.ijrobp.2012.10.017.
[64] Tan S, Zhang H, Zhang Y, Chen W, D'Souza WD, Lu W. Predicting pathologic tumor response to chemoradiotherapy with histogram distances characterizing longitudinal changes in 18F-FDG uptake patterns. Med Phys 2013;vol. 40(10):101707 ([Online]. Available), ⟨https://www.ncbi.nlm.nih.gov/pmc/articles/PMC3785537/pdf/MPHYA6-000040-101707_1.pdf⟩.
[65] Zhang H, et al. Modeling pathologic response of esophageal cancer to chemoradiation therapy using spatial-temporal 18F-FDG PET features, clinical parameters, and demographics. Jan 1 Int J Radiat Oncol Biol Phys 2014;vol. 88(1):195–203. https://doi.org/10.1016/j.ijrobp.2013.09.037.
[66] Lococo F, et al. 18F-fluorodeoxyglucose positron emission tomographic scan in solid-type p-stage-I pulmonary adenocarcinomas: what can produce false-negative results?. Apr 1 Eur J Cardiothorac Surg 2017;vol. 51(4):667–73. https://doi.org/10.1093/ejcts/ezw394.
[67] Austin JH, et al. Radiologic implications of the 2011 classification of adenocarcinoma of the lung. Radiology 2013;vol. 266(1):62–71. https://doi.org/10.1148/radiol.12120240.
[68] Rodriguez EF, Monaco SE, Dacic S. Cytologic subtyping of lung adenocarcinoma by using the proposed International Association for the Study of Lung Cancer/American Thoracic Society/European Respiratory Society (IASLC/ATS/ERS) adenocarcinoma classification. Cancer Cytopathol 2013;vol. 121(11):629–37. https://doi.org/10.1002/cncy.21314.
[69] Rudomina DE, Lin O, Moreira AL. Cytologic diagnosis of pulmonary adenocarcinoma with micropapillary pattern: does it correlate with the histologic findings? Diagn Cytopathol 2009;vol. 37(5):333–9. https://doi.org/10.1002/dc.21011.
[70] Yang SM, et al. Extraction of radiomic values from lung adenocarcinoma with near-pure subtypes in the International Association for the Study of Lung Cancer/the American Thoracic Society/the European Respiratory Society (IASLC/ATS/ERS) classification. Lung Cancer (Amst, Neth) 2018;vol. 119:56–63. https://doi.org/10.1016/j.lungcan.2018.03.004.